

Sarma phase in relativistic and non-relativistic systems

I. Boettcher,¹ T. K. Herbst,¹ J. M. Pawłowski,^{1,2} N. Strodtthoff,¹ L. von Smekal,^{3,4} and C. Wetterich^{1,2}

¹*Institute for Theoretical Physics, Heidelberg University, D-69120 Heidelberg, Germany*

²*ExtreMe Matter Institute EMMI, GSI Helmholtzzentrum für Schwerionenforschung mbH, D-64291 Darmstadt, Germany*

³*Theoriezentrum, Institut für Kernphysik, TU Darmstadt, D-64289 Darmstadt, Germany*

⁴*Institut für Theoretische Physik, Justus-Liebig-Universität, D-35392 Giessen, Germany*

(Dated: September 11, 2018)

We investigate the stability of the Sarma phase in two-component fermion systems in three spatial dimensions. For this purpose we compare strongly-correlated systems with either relativistic or non-relativistic dispersion relation: relativistic quarks and mesons at finite isospin density and spin-imbalanced ultracold Fermi gases. Using a Functional Renormalization Group approach, we resolve fluctuation effects onto the corresponding phase diagrams beyond the mean-field approximation. We find that fluctuations induce a second-order phase transition at zero temperature, and thus a Sarma phase, in the relativistic setup for large isospin chemical potential. This motivates the investigation of the cold atoms setup with comparable mean-field phase structure, where the Sarma phase could then be realized in experiment. However, for the non-relativistic system we find the stability region of the Sarma phase to be smaller than the one predicted from mean-field theory. It is limited to the BEC side of the phase diagram, and the unitary Fermi gas does not support a Sarma phase at zero temperature. Finally, we propose an ultracold quantum gas with four fermion species that has a good chance to realize a zero-temperature Sarma phase.

PACS numbers: 05.10.Cc, 11.10.Hi, 67.85.Lm

I. INTRODUCTION

Understanding the pairing mechanisms in fermionic many-body systems is a key step towards bridging the gap between microscopic models and macroscopic phenomena. A particularly interesting question concerns the stability of superfluidity in the presence of mismatching Fermi surfaces. Such an asymmetry between the pairing partners is realized in electronic materials in an external magnetic field [1–5], and is expected to be found in neutron stars [6–11]. With ultracold atoms this situation can easily be simulated by introducing a population imbalance between different hyperfine states. In a relativistic, QCD-related setting, non-vanishing isospin chemical potential similarly introduces an imbalance between different quark flavors, up and down. Alternatively, we may consider the relativistic isospin chemical potential as maintaining a balance between up and anti-down quarks with pairing in a superfluid pion condensate. The pair-breaking population imbalance is then introduced by the symmetric quark or baryon chemical potential.

While it is not possible to study, for example, the pairing mechanisms in neutron stars in table-top experiments, the high experimental control and accessibility of ultracold quantum gases makes them ideal setups to shed new light on superfluidity and its breakdown [12–16]. In particular, preparations of the spin-imbalanced BCS-BEC crossover allow the tuning of system parameters almost at will [17–23]. It is then interesting to study whether there is a parameter regime of the non-relativistic model that corresponds to a system relevant for nuclear or possible quark matter at high densities. Apart from the physical similarities of these systems, a positive answer to this question is expected based on the

observation that the mean-field phase diagrams in both cases look strikingly similar. To reach a conclusive statement, however, fluctuations beyond the mean-field approximation need to be taken into account, which is the aim of the present work.

In connection with the breakdown of superfluidity, the possible existence of a so-called Sarma phase [3] has gained a lot of interest recently [24–41]. The Sarma phase is a homogeneous superfluid phase with gapless fermionic excitations. To understand its origin we consider a gas of two species of fermions, labelled by an effective “spin” 1 and 2, with a chemical potential imbalance $\delta\mu = (\mu_1 - \mu_2)/2 \geq 0$ between them. After including renormalization effects on the propagator of fermionic quasiparticles, we can infer their dispersion relation from the quadratic part of the spin-imbalanced effective Lagrangian. It typically splits into two lowest branches given by

$$E_p^{(\pm)} = \sqrt{\varepsilon_p^2 + \Delta^2} \pm \delta\mu, \quad (1)$$

where ε_p is the microscopic dispersion relation of particles, and Δ is the pairing gap.

A Sarma phase is characterized by a non-vanishing gap Δ and the parameters in Eq. (1) are tuned such that the lower branch becomes negative in a momentum interval $p_{\min} < p < p_{\max}$, see Fig. 1. Accordingly, this interval becomes occupied even at zero temperature, and we find gapless excitations around the built-up Fermi surfaces at p_{\min} and p_{\max} . For the remaining momenta, fermionic excitations are gapped. For non-zero temperature the Fermi surfaces are smeared out and a sharp distinction between the unpolarized superfluid and the Sarma phase is not possible. Hence, we speak of a Sarma crossover in this case. The Sarma phase, or special cases of it, is

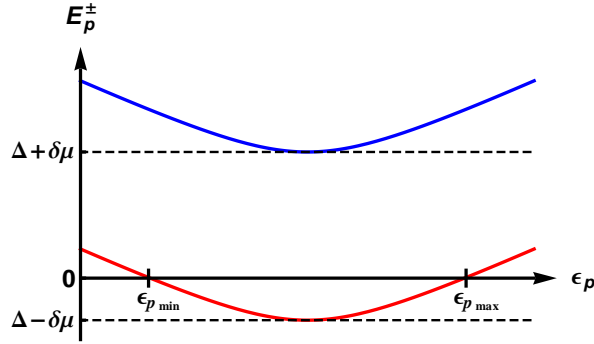


FIG. 1. The two lowest branches of the dispersion relation, Eq. (1), relevant for the Sarma transition. Increasing the imbalance $\delta\mu$, the lowest branch extends below zero, yielding gapless excitations around the Fermi surfaces at the corresponding momenta p_{\min} and p_{\max} . Note that for $\min_p \epsilon_p > 0$ the minimal $\epsilon_{p_{\min}}$ can become negative, and the Sarma phase appears with only one Fermi surface in this case.

also referred to as interior gap superfluid, breached pair phase, or magnetized superfluid in the literature.

The criterion for a zero crossing of the lower branch in Eq. (1), and thus for the onset of the Sarma phase, is equivalent to

$$\delta\mu > \min_p \sqrt{\epsilon_p^2 + \Delta^2}. \quad (2)$$

We emphasize again that this equation is understood in terms of renormalized single-particle quantities. Assuming for simplicity that $\min_p \epsilon_p = 0$, we then arrive at the condition $\delta\mu > \Delta$. Then there are three possible scenarios for a spin-imbalanced system with $\Delta > 0$, which decide over the fate of the Sarma phase. By increasing $\delta\mu$, we make pairing less favorable, and superfluidity generically breaks down at a critical imbalance $\delta\mu_c$. If this happens continuously, i.e. by means of a second-order phase transition, the Sarma criterion is necessarily fulfilled somewhere, since $\Delta \rightarrow 0$ (scenario I). This is depicted by the blue, dot-dashed line in Fig. 2. At a first-order phase transition, on the other hand, the gap jumps from a critical value $\Delta_c > 0$ to zero. For $\delta\mu_c > \Delta_c$ a Sarma phase exists (scenario II; red, dashed line in Fig. 2), whereas the required condition cannot be fulfilled for $\delta\mu_c < \Delta_c$ (scenario III; green, solid line). We see that the existence of a Sarma phase at a second-order transition line is a universal feature, whereas it becomes non-universal in the vicinity of a first-order transition line.

In experiments with ultracold atoms the Sarma phase can be inferred from a non-monotonous or non-continuous momentum distribution after time-of-flight expansion [41]. At non-zero temperature, the sharp features in the momentum distribution are smeared out. The Sarma phase also shows up in shell-structured in-situ density images, where the polarized superfluid manifests itself in a population imbalance between the spin species [31]: If the transition to the normal gas is of first order,

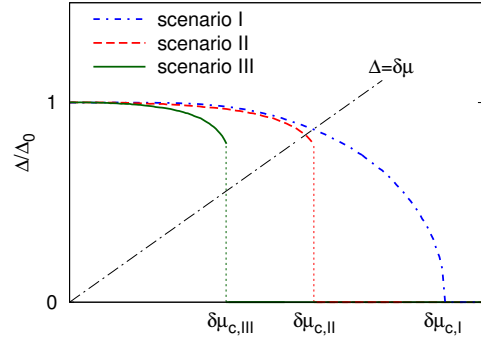


FIG. 2. The three possible scenarios for the Sarma condition $\Delta = \delta\mu$; see discussion below Eq. (2) for details. In the case of a second-order superfluid phase transition the criterion is always fulfilled for some $\delta\mu$ (Scenario I), whereas the size of the critical gap at a first-order transition decides whether it is fulfilled (Scenario II) or not (Scenario III).

an intermediate population imbalanced superfluid region in the cloud which smoothly connects to the balanced superfluid, indicates the Sarma phase. If the transition is of second order, the superfluidity of the population imbalanced region can be probed by the excitation of vortices. The presence of Fermi surfaces is also expected to induce metallic features in the superfluid, which are observable in its transport properties. This makes the system an unconventional superfluid. The transport properties of neutron stars are known to be closely linked to their constitution and life time. A possible Sarma phase is thus of relevance for interpreting the stellar evolution.

As discussed above, the two systems studied in the following look very similar at first glance and indeed it is found that their mean-field phase diagrams agree qualitatively. Upon closer inspection, however, especially the bosonic sectors of the two theories differ. Fluctuation contributions from this sector are not accounted for in a mean-field approximation, but may lead to strong modifications of the phase diagram. Notably, the relativistic system shows a richer phase structure, including a Sarma phase at low temperature once fluctuations are taken into account, see Sec. II. One can then ask whether this is also true in the non-relativistic setting, where such additional phases are potentially accessible in experiment.

To study spin-imbalanced systems beyond the mean-field approximation, we employ the Functional Renormalization Group (FRG), which enables the systematic inclusion of fluctuations. In particular, it naturally incorporates the feedback of order parameter fluctuations onto the full effective potential. As a consequence, physical observables show the correct beyond mean-field scaling at second-order phase transitions. Additionally, the FRG is free of the sign problem, which hampers Quantum Monte Carlo studies of spin-imbalanced systems [42]. Hence, the full phase diagrams of both the spin-imbalanced non-relativistic and the isospin-asymmetric relativistic system are accessible. For extensive reviews on the method

see Refs. [43–50]. Comprehensive introductions to the FRG approach for QCD-like models and the BCS-BEC crossover, respectively, can be found in Refs. [51, 52] and [53, 54].

To highlight the impact of bosonic fluctuations, we compare results in the mean-field approximation to those obtained with the FRG. In many cases, mean-field theory predicts a first-order breakdown of superfluidity due to spin-imbalance at $T = 0$. Including fluctuations, this first-order transition can turn into a continuous one. This interesting effect has indeed been found in FRG studies of two-dimensional Hertz–Millis type actions [55], and a non-relativistic spin-imbalanced Fermi gas on the BCS-side of the crossover in two spatial dimensions [56]. In the present analysis we find such a smoothing of the transition in the relativistic model, whereas it is absent in the non-relativistic setting.

This paper is organized as follows. In Sec. II we consider the relativistic system, where bosonic fluctuations induce a Sarma phase close to the breakdown of charged pion condensation at zero temperature. We then consider the non-relativistic analog in Sec. III. After discussing our approximation we investigate the stability of the Sarma phase in the unitary Fermi gas at zero and finite temperature, and then turn to the imbalanced BCS-BEC crossover at zero temperature. We draw our conclusions in Sec. IV.

II. RELATIVISTIC SYSTEM

In this section we investigate the fate of the Sarma phase in a relativistic system. To this end, we employ a quark-meson model, which is frequently used as a low-energy effective model for QCD, with quarks and mesons as effective degrees of freedom [57–62]. Here we introduce both a finite quark, μ_q , and isospin, μ_I , chemical potential. The quark chemical potential, defined as one third of the baryon chemical potential, induces an imbalance between quarks and anti-quarks. In contrast, the isospin chemical potential induces an imbalance between the quark flavors, up and down. Similar to the non-relativistic case discussed in Sec. III, this setup allows to study the impact of mismatched Fermi spheres on fermion pairing. In fact, at low temperature and finite densities, the system describes a superfluid in the BCS-BEC crossover [63], similar to the non-relativistic case discussed below: At moderately large $|\mu_I| > m_\pi/2$ charged pions condense and form a Bose condensate. The ground state then is a superfluid of pions. In the limit of large $|\mu_I|$, on the other hand, Cooper-pairing between quarks and antiquarks sets in. Also in this case the relevant channel carries the quantum numbers of a pion. Hence we expect a smooth crossover from BEC- to BCS-like pairing as μ_I is increased.

Moreover, the case of a pure isospin chemical potential, i.e. vanishing quark chemical potential, is one example for a QCD-like theory without a fermion sign problem.

The latter represents the main obstacle for studying the phase diagram of QCD at finite quark chemical potential using Lattice Monte Carlo methods [64]. However, the situation of both, a finite quark and finite isospin chemical potential, is also of direct physical interest in the context of heavy ion collisions or quark matter inside neutron stars.

The omission of a possible diquark condensate and the absence of baryonic degrees of freedom constitute natural limitations of the capability of this model to describe QCD at high densities. Here, however, we are mainly interested in the similarities of this relativistic model with its non-relativistic counterpart discussed below. Hence, such QCD-related limitations are of no concern for the present work.

The model is described by a Lagrangian of the form [65]

$$\mathcal{L} = \bar{\psi} (\not{d} + g(\sigma + i\gamma^5 \vec{\pi} \cdot \vec{\tau}) - \gamma_0 \mu_q - \gamma_0 \tau_3 \mu_I) \psi + \frac{1}{2} (\partial_\nu \sigma)^2 + \frac{1}{2} (\partial_\nu \pi_0)^2 + U(\chi, \rho) - c\sigma + \frac{1}{2} (\partial_\nu + 2\mu_I \delta_\nu^0) \pi_+ (\partial_\nu - 2\mu_I \delta_\nu^0) \pi_-, \quad (3)$$

where τ_i denote Pauli matrices in flavor space and we define invariants $\chi \equiv \sigma^2 + \pi_0^2$ (with $\pi_0 \equiv \pi^3$), $\rho \equiv \pi_+ \pi_-$ (with $\pi_\pm = \pi_1 \pm i\pi_2$) and $\psi = (\psi_u, \psi_d)^T$. The four (real) bosonic degrees of freedom are given by the isospin-singlet (σ) and -triplet ($\vec{\pi}$), which combine to a four-component (2, 2) representation of the chiral $SU(2)_L \times SU(2)_R$ symmetry of the theory.

At finite isospin chemical potential the effective potential in general is a function of both invariants χ and ρ . Its minimum (χ_0, ρ_0) determines the phase structure of the system, where a finite value of $\chi_0 = \langle \chi \rangle$ signals broken chiral symmetry and a finite value of $\rho_0 = \langle \rho \rangle$ signals a phase of charged pion condensation. This value can then be used to define the gap parameter as $\Delta^2 \equiv g^2 \rho_0$. The following analysis focuses on the charged pion condensation phase and its disappearance with increasing quark chemical potential.

Within the framework of the FRG we investigate the model Eq. (3) in the local potential approximation (LPA), where only a scale-dependent effective potential is considered. However, the full field dependence of the effective potential is taken into account by expanding it on a two-dimensional grid in field space [66]. For a comprehensive description of the phase structure of this model as a function of the three external parameters (T, μ_q, μ_I) as obtained with the FRG, as well as for a more detailed description of the truncation and implementation, we refer the reader to [65]. Here we only briefly recapitulate the features most relevant for the present investigation.

For sufficiently large isospin chemical potential and sufficiently small quark chemical potential there is a phase of charged pion condensation. At zero temperature the phase diagram is strongly constrained by the Silver Blaze property [65, 67], which prohibits a dependence of the partition function on the chemical potential until the latter exceeds the mass of the lowest excitation it cou-

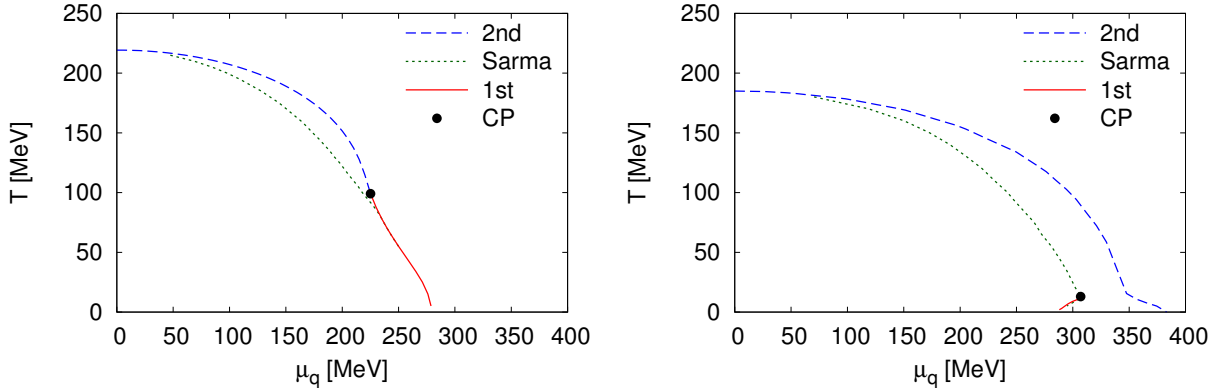


FIG. 3. Phase structure of the quark-meson model for $\mu_I = m_\pi$ in mean-field approximation (MFA, left) and from the FRG (right). The Sarma phase occurs in the region between the dotted and dashed lines. While the MFA result looks very similar to the one of the UFG, cf. Fig. 4, the FRG result features a Sarma phase at $T = 0$.

ples to. At vanishing quark chemical potential for example, this entails that the onset of pion condensation is found at $\mu_I = m_\pi/2$. At fixed $\mu_I > m_\pi/2$ with increasing quark chemical potential μ_q the charged pion condensation phase finally breaks down. Interestingly, for $\mu_I > 0.79m_\pi$ the full calculation including bosonic fluctuations shows an additional first-order transition at small and vanishing temperatures inside the pion condensation phase close to its phase boundary [65].

One possible interpretation for this transition is a first-order transition to a Sarma phase, corresponding to scenario II in Fig. 2, and hence the existence of a stable Sarma phase at vanishing temperature. As outlined above, the definition of the Sarma phase relies on the notion of quasiparticle dispersion relations, which, for the Lagrangian given in Eq. (3), take the form

$$\varepsilon_p = \sqrt{\vec{p}^2 + m_\psi^2} - \mu_I, \quad (4)$$

where $m_\psi^2 = g^2\chi$. For $\mu_I > m_\psi$ we have $\min_p \varepsilon_p = 0$ [65, 68], and the criterion for the stability of the Sarma phase, Eq. (2), reduces to $\Delta < \mu_q$. In particular, this is true in the case of restored chiral symmetry. To investigate the appearance of a Sarma phase in more detail, we study slices of the three-dimensional phase diagram at a fixed value of $\mu_I = m_\pi$. As remarked above, for this value a first-order transition inside the pion condensation occurs upon increasing μ_q . Estimating the location of the BCS-BEC crossover via the simple criterion of the zero-crossing of $\min_p \varepsilon_p$, i.e. $\mu_I = m_\psi$, translates into a value of $0.82m_\pi$. Hence the choice $\mu_I = m_\pi$ corresponds to a point just on the BCS-side of the crossover.

The corresponding $(\mu_I - T)$ -phase diagrams are shown in Fig. 3, where the left panel shows the outcome of a mean-field calculation which can be obtained in a consistent way from the FRG by including only fermionic contributions to the flow, cf. Sec. III B below. For small temperatures the boundary of the pion condensation phase is a first-order transition line. This is the

analog of the Chandrasekhar–Clogston transition [1, 2] in non-relativistic Fermi gases. It turns second order for larger temperatures in a multicritical point which could become a Lifshitz point if inhomogeneous Fulde–Ferrell–Larkin–Ovchinnikov phases occur [4, 5, 23, 69, 70]. This situation is analogous to the inhomogeneous phases discussed for chiral symmetry restoration at finite baryon chemical potential in QCD, for a recent review see [71]. As outlined in the introduction, the second-order transition line at larger temperatures is accompanied by a stable Sarma phase. The Sarma phase, however, does not extend to the zero temperature axis, because the Chandrasekhar–Clogston limit is reached before a possible Sarma transition could occur at low temperatures in the mean-field calculation.

In contrast, the right panel of Fig. 3 shows the full result including bosonic fluctuations in LPA. Here the phase boundary of the pion condensation phase remains second order throughout the whole phase diagram. However, an additional first-order transition arises inside the pion condensation phase. As the condensate jumps to a sufficiently low value across the phase boundary, the Sarma criterion is satisfied. Therefore, unlike in the mean-field calculation, the Sarma phase now extends down to zero temperature in the calculation including bosonic fluctuations. As discussed above, mean-field studies of chiral systems, however, suggest that the phase structure at low temperature is altered once inhomogeneous phases are taken into account. This effect may persist when fluctuations are included, but for the system under consideration no results are available thus far. In fact, the study of inhomogeneous phases beyond MFA poses a sophisticated task, see e.g. [72, 73] for recent developments within the FRG. For instance, within a derivative expansion the vanishing of the bosonic wave function renormalization may signal the onset of inhomogeneous condensation [72].

Furthermore, on the mean-field level, the phase dia-

grams of the relativistic system, Fig. 3 (left), and the unitary Fermi gas (UFG), Fig. 4 (upper lines), look strikingly alike. In fact, the phase structure of the imbalanced Unitary Fermi Gas has become experimentally accessible by now. The existence of a similar Sarma phase at low T in the non-relativistic system could hence be checked experimentally. This serves as our motivation to include fluctuations in the non-relativistic system and study its phase structure in Sec. III below.

III. NON-RELATIVISTIC SYSTEM

As the non-relativistic realization of the system under consideration, we study a system of ultracold two-component fermions close to a broad Feshbach resonance (FR). Its description in terms of the two-channel model is built on a Grassmann field ψ_σ , one complex bosonic field ϕ and the microscopic Lagrangian [13, 16, 74]

$$\begin{aligned} \mathcal{L} = & \sum_{\sigma=1,2} \psi_\sigma^* \left(\partial_\tau - \frac{\nabla^2}{2M_\sigma} - \mu_\sigma \right) \psi_\sigma - g \left(\phi^* \psi_1 \psi_2 + \text{h.c.} \right) \\ & + \phi^* \left(Z_\phi \partial_\tau - A_\phi \frac{\nabla^2}{4M} \right) \phi + \nu_\Lambda \phi^* \phi. \end{aligned} \quad (5)$$

The two species of fermions couple to chemical potentials μ_σ , which in general are different. We assume the 1-atoms to be the majority species and write

$$\mu_1 = \mu + \delta\mu, \quad \mu_2 = \mu - \delta\mu, \quad (6)$$

with spin-imbalance $\delta\mu = h = (\mu_1 - \mu_2)/2 \geq 0$. The quantity h is also referred to as Zeeman field. We assume mass balance in the following and choose units such that $\hbar = k_B = 2M_\sigma = 2M = 1$ for the non-relativistic analysis.

The parameter $\nu_\Lambda \propto (B - B_0)$ is related to the detuning from the FR, and eventually allows the computation of the s-wave scattering length, a , of the system. The Feshbach coupling $g^2 \propto \Delta B$ corresponds to the width of the FR. We assume the FR to be broad in the following, such that the two-channel model in Eq. (5) is equivalent to a single-channel model of fermions.

The self-interaction of the bosonic degree of freedom is encoded in the effective potential, $U(\rho = \phi^* \phi)$. At the microscopic scale we have $U(\rho) = \nu_\Lambda \rho$, but the ρ -dependence is changed substantially when including fluctuations. In the following, we compute the effective potential $U(\rho)$ beyond the mean-field approximation with feedback of bosonic fluctuations. The minimum position of this potential, ρ_0 , is related to the superfluid density and acts as an order parameter for the superfluid-to-normal phase transition. For convenience, and similar to the relativistic case, we use the gap $\Delta_0^2 = g^2 \rho_0$, rather than ρ_0 itself as the order parameter.

Note that the binding energy $\varepsilon_B < 0$ is non-zero on the BEC side, and the fermion chemical potential eventually becomes negative for large positive scattering length. By

contrast, we set $\varepsilon_B = 0$ on the BCS side. The quantity $\tilde{\mu} = \mu - \varepsilon_B/2 > 0$ is manifestly positive for non-vanishing density, and we choose units such that $\tilde{\mu} = 1$ when discussing the whole crossover. A negative chemical potential shifts the minimum in the Sarma criterion Eq. (2). Taking this possibility into account, the criterion generalizes to

$$\delta\mu > \min_p \sqrt{\varepsilon_p^2 + \Delta_0^2} = \begin{cases} \Delta_0, & (\mu \geq 0) \\ \sqrt{\mu^2 + \Delta_0^2}, & (\mu < 0) \end{cases}. \quad (7)$$

A. Relation to the Relativistic Model

As we have argued above, the relativistic system Eq. (3) and the non-relativistic one, Eq. (5), both describe two-component fermionic systems in the BCS-BEC crossover. Actually, the Lagrangian Eq. (3) can be seen as the relativistic analog of Eq. (5): on a very basic level both represent a Yukawa system with fermions coupled to two different chemical potentials. To be precise, $\delta\mu$ in the non-relativistic case should be identified with the quark chemical potential μ_q , whereas the chemical potential μ in the non-relativistic case corresponds to the isospin chemical potential μ_I . To simplify the comparison we provide a dictionary between the two systems in Tab. I.

On closer inspection, though, the field content of the models is different: the relativistic spinor is subject to an additional chiral symmetry, under which the left- and right-handed components, $\psi_{R/L} = \frac{1}{2}(1 \pm \gamma_5)\psi$, transform separately. The four (real) bosonic degrees of freedom, transforming as singlet and triplet under isospin rotations, are related to these components in the following way

$$\begin{aligned} \pi_+ &\sim u_L d_L^\dagger + u_R d_R^\dagger, \\ \pi_- &\sim d_L u_L^\dagger + d_R u_R^\dagger, \\ \pi_0 &\sim u_L u_L^\dagger + u_R u_R^\dagger - (u \rightarrow d), \\ \sigma &\sim u_L u_R^\dagger + u_R u_L^\dagger + (u \rightarrow d), \end{aligned}$$

where we have used the notation $u := \psi_u$ and $d := \psi_d$ for better readability. Using the correspondence $\psi_1 \leftrightarrow u$ and $\psi_2 \leftrightarrow d^\dagger$, it is clear that $\pi_+ \leftrightarrow \phi$ and $\pi_- \leftrightarrow \phi^*$. The other two bosonic degrees of freedom, π_0 and σ , however, have no counterpart in the non-relativistic system. They reflect the larger symmetry group, $SU(2) \times SU(2)$, of the relativistic system. Owing to this discrepancy, one can expect that the impact of bosonic fluctuations on the relativistic and non-relativistic systems is different. Furthermore, the fields u, d^\dagger each describe two independent fermions u_L, u_R and d_L^\dagger, d_R^\dagger , respectively, while ψ_1 and ψ_2 account only for a single fermion.

Other than that, the condensation of charged pions in Eq. (3) is the equivalent of the di-fermion condensation occurring in the non-relativistic system. The related order parameter in both cases is the gap Δ . Note that

non-relativistic	relativistic	interpretation
ψ_1, ψ_2	ψ_u, ψ_d^\dagger	spin/flavor eigenstates
μ	μ_I	induces pairing
$\delta\mu$	μ_q	knob to destroy pairing
$\delta n = n_1 - n_2$	$\delta n = n_q - n_{\bar{q}}$	population imbalance
$\Delta^2 = g^2 \phi^* \phi$	$\Delta^2 = g^2 \pi_+ \pi_-$	pairing order parameter
-	χ	chiral condensate

TABLE I. Dictionary between quantities in the non-relativistic and relativistic system and their interpretation.

also the universal aspects of a second-order condensation transition agree: the condensate Δ always breaks a $U(1)$ symmetry.

B. FRG Setting and Truncation

To investigate the stability of the Sarma phase in the spin-imbalanced BCS-BEC crossover we employ the FRG approach described in [75, 76]. We refer to those references for a detailed discussion of the truncation and regularization scheme. Here we only summarize the main features which are relevant for the present analysis.

To properly account for first-order phase transitions and the competition of multiple minima one needs to know the effective potential $U(\rho)$ over a large range of ρ -values. For this purpose we discretize the potential on a grid in the gap $\Delta = g^2 \rho$. Alternative approaches are based on higher-order Taylor expansions of the effective potential around a fixed value [77], or the expansion in terms of suitable basis functions. Note that a recent analysis of the BCS side in [78] is built on a Taylor expansion of $U(\rho)$ to order ρ^2 , as thus fails to resolve the first-order transition in the perturbative Clogston limit [1, 2]. Furthermore, we want to remark that the FRG approach allows to recover the mean-field result in a conceptually consistent way: neglecting the bosonic contributions to the flow equations, the standard mean-field result is reproduced [75, 79, 80].

From mean-field studies of the phase structure of the imbalanced UFG [31, 32, 35], we expect a first-order phase transition at low temperatures. This suggests that the stability of the Sarma phase at zero temperature is decided according to Scenarios II and III from above. To distinguish between these two scenarios, renormalization effects on Δ_c and $\delta\mu$ are expected to be important. In the present work, we introduce a single wave function renormalization, A_ϕ , for the bosonic field and set $A_\phi = Z_\phi$ in Eq. (5). We do not include the particle-hole correction to the four-fermion vertex or the renormalization of the fermion propagator. Those contributions have been shown to be subleading for the phase structure of the balanced system with the FRG [80–84]. Here we discuss why we expect them to be subleading for the discussion of the existence of the Sarma phase as well.

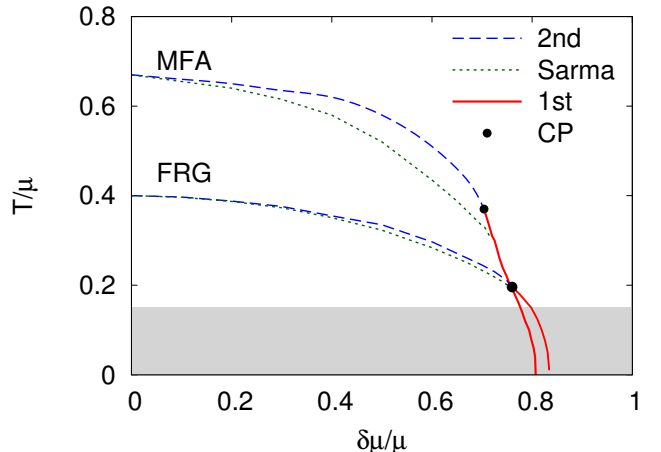


FIG. 4. Phase structure of the imbalanced unitary Fermi gas. The upper lines correspond to the mean-field approximation (MFA), the lower ones to the FRG result. We observe a substantial decrease in the critical temperature due to bosonic fluctuations. The Sarma condition $\Delta = \delta\mu$ is fulfilled along the dotted green line close to the second-order phase boundary. Interestingly, in both cases we do not find a Sarma phase at zero temperature.

From studies of the polaron [38, 85, 86] and the balanced UFG [80] it is known that fluctuation effects tend to *increase* the individual chemical potential, μ_σ , by a contribution approximately proportional to the chemical potential of the other species, $\mu_{\bar{\sigma}}$. In both cases, fluctuations induce renormalization effects on the order of 60%,

$$\mu_{\sigma,\text{eff}} \simeq \mu_\sigma + 0.6 \mu_{\bar{\sigma}}. \quad (8)$$

Assuming this relation to be generally valid, we can estimate the effective imbalance to be given by

$$\delta\mu_{\text{eff}} = (\mu_{1,\text{eff}} - \mu_{2,\text{eff}})/2 \simeq 0.4 \delta\mu, \quad (9)$$

i.e. the effective imbalance is smaller than the unrenormalized (or bare) one. The Sarma criterion $\Delta_c < \delta\mu_{\text{eff}}$, which has to be true for the renormalized (or dressed) parameters, is even less likely fulfilled. In particular, for most cases discussed below we find that the Sarma criterion is violated already for the unrenormalized imbalance. According to our argument here, this implies that it is also violated for the renormalized one.

C. Unitary Fermi Gas

Motivated by the similarity of its mean-field phase diagram to the relativistic system discussed in Sec. II, we start our discussion with the imbalanced UFG, where the superfluid is strongly correlated.

The mean-field phase structure is recovered by neglecting bosonic fluctuations in the FRG flow equation. This

is demonstrated in Fig. 4 (upper lines labelled “MFA”). We find a second-order phase transition (blue, long-dashed line) for $\delta\mu = 0$ in agreement with the expectation from the balanced BCS-BEC crossover. The related mean-field critical temperature is $T_c/\mu = 0.665$. In the imbalanced case we observe a first-order transition (red, solid line) from the superfluid to the normal phase at $\delta\mu_c/\mu = 0.807$ at zero temperature. The critical point, separating the first- from the second-order transition line, is found at $(\delta\mu_{\text{CP}}/\mu, T_{\text{CP}}/\mu) = (0.704, 0.373)$. These results are in line with the literature [32, 35]. The Sarma phase (green, dotted line) appears in the vicinity of the second-order transition line. Note that the dotted green line, corresponding to the condition $\Delta = \delta\mu$, only serves as an orientation, since the transition is a crossover at non-zero temperature. The Sarma crossover line terminates close to the critical point, where it hits the first-order transition. The jump in the gap then prevents the Sarma condition from being fulfilled for lower temperatures. This corresponds to Scenario III discussed above. We conclude that, at the mean-field level, there is no stable Sarma phase at $T = 0$.

Next we include the feedback of bosonic fluctuations. The resulting phase diagram is also shown in Fig. 4 (lower lines labelled “FRG”). At vanishing imbalance we again find a second-order phase transition. The transition temperature, however, is drastically reduced to $T_c/\mu = 0.40$. Overall, the inclusion of bosonic fluctuations makes the transition sharper, resulting in a *shrinking* Sarma phase. Furthermore, this phase appears at relatively high temperatures only. In this regime the presence of gapless fermionic excitations is smeared out, and may be difficult to detect in experiment.

At vanishing temperature we still find a first-order transition with a critical imbalance of $\delta\mu_c/\mu = 0.83$. This is larger than the mean-field prediction, and in reasonably good agreement with the recent experimental finding $\delta\mu_c/\mu = 0.89$ [87]. The latter reference also confirms the first-order phase transition at low temperatures.

Note that, due to its complexity, it is hard to evolve the FRG flow for very small k in the low temperature region. A conservative estimate for the latter is indicated by the grey band in Fig. 4. The determination of the phase boundary, however, is still reliable in this region. A more detailed discussion of this point is provided in [75]. Furthermore, the critical point, the onset of the first-order transition and the end of the Sarma phase all lie well above this band. Hence we can draw our conclusions independent of this limitation.

D. BCS-BEC crossover

Our initial motivation to study the fate of the Sarma phase at low temperatures upon inclusion of fluctuations was the claim that the relativistic system discussed in Sec. II agrees with the UFG on the mean-field level. However, the mean-field phase diagrams throughout the BCS-

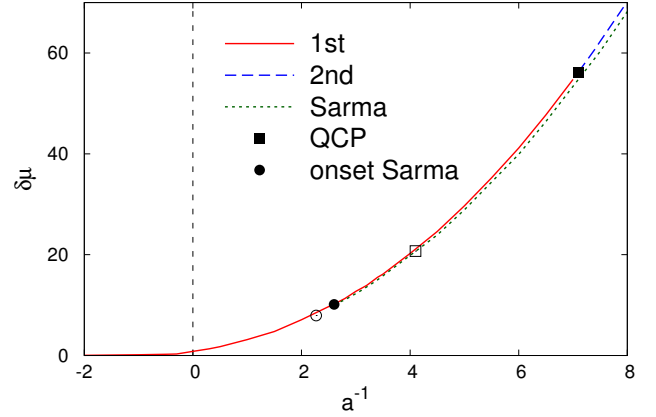


FIG. 5. Quantum phase diagram of the imbalanced BCS-BEC crossover from the FRG. Units are chosen such that $\tilde{\mu} = \mu - \epsilon_B/2 = 1$. The first-order superfluid phase transition appearing on the BCS side persists on the BEC side up to the quantum critical point (QCP). The QCP is marked by a filled (open) square for the result from the FRG (mean-field) analysis. The onset of the Sarma phase along the first-order line according to Scenario II is indicated by the filled (open) circle for the FRG (mean-field) result. The boundary of the Sarma phase on the BEC side is given by the dotted green line.

BEC crossover look very similar, apart from a change of scales. Moreover, the simple estimate presented in Sec. II suggests that the relativistic phase diagram shown there rather corresponds to a point on the BCS side of the crossover. Hence we extend our study to finite scattering lengths (the only tunable parameter in this system) in order to identify a region that might support a stable Sarma phase at $T = 0$. Additionally we want to note that even the phase structure of the imbalanced BCS-BEC crossover beyond mean-field had been unknown to a large extent so far.

In the following we focus on the phase structure of the imbalanced BCS-BEC crossover at zero temperature, i.e. the quantum phase diagram. The mean-field result has previously been calculated in, e.g., [30, 32, 35]. The superfluid-to-normal transition is of first order on the BCS side ($a^{-1} < 0$). This behavior persists on the BEC side ($a^{-1} > 0$) up to a quantum critical point (QCP) where the transition turns to second order. Within the mean-field approximation, the QCP is located at

$$(\sqrt{\tilde{\mu}}a)^{-1}_{\text{MF}} = 4.19, \quad \delta\mu_{\text{MF}} = 21.6\tilde{\mu} = 0.61|\epsilon_B|.$$

We again employ the definition $\tilde{\mu} = \mu - \epsilon_B/2$.

The quantum phase diagram including the feedback of bosonic fluctuations from Functional Renormalization is shown in Fig. 5. Its structure is even quantitatively very similar to the mean-field result, hence we only show the FRG result and have superimposed the locations of the QCP and the onset of the Sarma transition from the

MFA. On the BCS side and in the vicinity of the resonance, the transition is of first order. On the BEC side there is a QCP where a second-order line emerges. Its coordinates read

$$(\sqrt{\tilde{\mu}a})_{\text{FRG}}^{-1} = 7.1, \quad \delta\mu_{\text{FRG}} = 56.2\tilde{\mu} = 0.56|\varepsilon_B|,$$

within our approximation. We see that, contrary to the relativistic case discussed above, fluctuations rather induce a first-order phase transition than a second order one.

The onset of the Sarma phase on the BEC side is located to the left of the QCP, and thus happens according to Scenario II in the terminology introduced above. The boundary of the Sarma phase according to Eq. (7) is indicated by the dotted green line in Fig. 5. It terminates in the first-order line at $(\sqrt{\tilde{\mu}a})_{\text{MF}}^{-1} = 2.27$ in MFA, which is shifted towards $(\sqrt{\tilde{\mu}a})_{\text{FRG}}^{-1} = 2.6$ when including bosonic fluctuations. To the right of the QCP we always find a stable Sarma phase below the second-order line, according to Scenario I. Since the Sarma phase only appears on the BEC side, the corresponding magnetized superfluid constitutes a homogeneous state consisting of a BEC of diatomic molecules with excess majority atoms.

Hence we find that our initial question for a parameter set that supports a Sarma phase at $T = 0$ including fluctuations, but not on the mean-field level, has to be answered negatively: the onset of the Sarma phase occurs at lower inverse scattering lengths in the MFA than with the FRG. In contrast, there is an, albeit small, window where the mean-field phase diagram shows a Sarma phase which vanishes after the inclusion of fluctuations. Moreover, as distinguished from the relativistic case, a Sarma phase arises only on the *BEC side* of the crossover in the non-relativistic system.

IV. CONCLUSIONS

Triggered by the close resemblance of the phase diagrams of relativistic and non-relativistic two-component fermion systems on the mean-field level, we have studied the fate of this similarity once fluctuations are taken into account.

We have studied the two-flavor quark-meson model coupled to quark as well as isospin chemical potentials as a relativistic realization of this system. Fixing the isospin chemical potential to a value that allows for pion condensation, $\mu_I > m_\pi/2$, one can study the breakdown of the related pion-superfluidity as the quark chemical potential is varied. In fact, on the mean-field level the resulting phase diagram looks remarkably similar to the one of the spin-imbalanced unitary Fermi gas, see Sec. III. Including fluctuations in the relativistic setting, the phase diagram changes drastically for $\mu_I \gtrsim 0.79m_\pi$: At low temperatures, the transition line splits into two branches, one of first and one of second order. Interestingly, the Sarma-crossover line meets the first-order transition in the critical point, while the second-order line continues down to

$T = 0$. This means that the relativistic system features a Sarma phase at $T = 0$.

The non-relativistic system under consideration, the spin-imbalanced BCS-BEC crossover of ultracold atoms, does not show this feature despite the apparent similarities in the mean-field phase structure of both system. While the location of the phase boundaries is modified by the inclusion of fluctuations, e.g. the critical temperature is drastically reduced, the general structure of the phase diagram persist. At unitarity, the unpolarized superfluid ground state at zero temperature is separated from the normal phase by a first-order phase transition. Moreover, the Sarma criterion (2) is not fulfilled at the phase boundary. Thus the superfluid with unequal densities $n_1 \neq n_2$ can only be realized as an inhomogeneous mixed state. The realization of a first-order phase transition is in agreement with the available experimental data.

Since the relativistic system considered in Sec. II presumably lies on the BCS side of the crossover, we have extended our non-relativistic study to the whole BCS-BEC crossover at low T . A zero temperature Sarma phase in the non-relativistic setup is only found on the BEC side of the crossover, close to the region predicted from mean-field theory. We were able to locate the QCP on the BEC side, where the transition changes from first to second order. An interesting question then concerns the critical exponents at the QCP on the BEC side, which can be computed with the FRG to high accuracy [88]. A more detailed analysis of the quantum critical properties of the QCP will be presented elsewhere.

Finally, as we have discussed in Sec. III A, there exist some crucial differences between the relativistic and non-relativistic systems under consideration: Due to the additional chiral symmetry, the relativistic system features effectively four species of fermions as well as four real bosonic degrees of freedom. Of these, the chirality-preserving but flavor-mixing combinations, corresponding to the bosonic fields π_\pm , are the counterparts of the complex non-relativistic boson ϕ . The presence of two additional bosonic modes, however, modifies the dynamics of the system substantially. In particular, it results in a Sarma phase at vanishing temperature in the relativistic theory that is not present in the non-relativistic setting. The agreement of the phase diagrams on the mean-field level, on the other hand, suggests that the differences in the fermionic sector are not as crucial.

Based on these observations, we can now suggest a non-relativistic system that resembles the relativistic one more closely. Such a system would be interesting to study both experimentally and theoretically, since it might feature a Sarma phase at $T = 0$, similar to the relativistic theory discussed above. For this purpose, one needs to study a system with four fermion species, $\psi_{1,2,3,4}$. Furthermore, interactions need to be tuned such that channels equivalent to the interactions in Eq. (3) are present and have similar interaction strengths. The corresponding microscopic Hamiltonian, which needs to be imple-

mented with cold atoms, reads

$$\hat{H} = \int d^3x \left[\sum_{\sigma=1}^4 \psi_{\sigma}^{\dagger} \left(-\frac{\nabla^2}{2M} - \mu_{\sigma} \right) \psi_{\sigma} + \lambda \left((\psi_1 \psi_2)^{\dagger} \psi_1 \psi_2 + (\psi_3 \psi_2)^{\dagger} \psi_3 \psi_2 + (\psi_1 \psi_4)^{\dagger} \psi_1 \psi_4 + (\psi_3 \psi_4)^{\dagger} \psi_3 \psi_4 \right) \right]. \quad (10)$$

The resulting system then possesses a chiral symmetry similar to the relativistic one, with $SU(2)_L$ acting on the doublet (ψ_1, ψ_3) and $SU(2)_R$ acting on (ψ_2, ψ_4) . The interaction involves particular combina-

tions of $n_{\alpha} = \psi_{\alpha}^{\dagger} \psi_{\alpha}$, namely $(n_1 + n_3)(n_2 + n_4)$. One could expect to find a similar phase structure as shown in Fig. 3, in particular a Sarma phase at $T = 0$.

ACKNOWLEDGEMENTS

The authors thank J. Braun and D. Roscher for valuable discussions and collaboration on related work. I. B. acknowledges funding from the Graduate Academy Heidelberg. L.v.S. is supported by the Helmholtz International Center for FAIR within the LOEWE program of the State of Hesse. This work is also supported by the Helmholtz Alliance HA216/EMMI and the grant ERC-AdG-290623.

[1] A. M. Clogston, Phys. Rev. Lett. **9**, 266 (1962).
[2] B. S. Chandrasekhar, Applied Physics Letters **1**, 7 (1962).
[3] G. Sarma, Journal of Physics and Chemistry of Solids **24**, 1029 (1963).
[4] P. Fulde and R. A. Ferrell, Phys. Rev. **135**, A550 (1964).
[5] A. Larkin and Y. Ovchinnikov, Zh.Eksp.Teor.Fiz. **47**, 1136 (1964).
[6] U. Lombardo and H. Schulze, Lect.Notes Phys. **578**, 30 (2001).
[7] D. J. Dean and M. Hjorth-Jensen, Rev. Mod. Phys. **75**, 607 (2003).
[8] M. G. Alford, A. Schmitt, K. Rajagopal, and T. Schäfer, Rev. Mod. Phys. **80**, 1455 (2008).
[9] D. Page, J. M. Lattimer, M. Prakash, and A. W. Steiner, (2013), arXiv:1302.6626 [astro-ph.HE].
[10] A. Gezerlis, C. Pethick, and A. Schwenk, (2014), arXiv:1406.6109 [nucl-th].
[11] T. Krüger, K. Hebeler, and A. Schwenk, (2014), arXiv:1408.4168 [nucl-th].
[12] W. Ketterle, D. Durfee, and D. Stamper-Kurn, Proceedings of the International School of Physics "Enrico Fermi", Course CXL, edited by M. Inguscio, S. Stringari and C.E. Wieman, 67 (1999).
[13] V. Gurarie and L. Radzihovsky, Annals of Physics **322**, 2 (2007).
[14] I. Bloch, J. Dalibard, and W. Zwerger, Rev. Mod. Phys. **80**, 885 (2008).
[15] S. Giorgini, L. P. Pitaevskii, and S. Stringari, Rev. Mod. Phys. **80**, 1215 (2008).
[16] W. Zwerger, ed., *The BCS-BEC Crossover and the Unitary Fermi Gas* (Springer, Berlin, 2012).
[17] G. B. Partridge, W. Li, R. I. Kamar, Y.-a. Liao, and R. G. Hulet, Science **311**, 503 (2006).
[18] M. W. Zwierlein, A. Schirotzek, C. H. Schunck, and W. Ketterle, Science **311**, 492 (2006).
[19] Y. Shin, M. W. Zwierlein, C. H. Schunck, A. Schirotzek, and W. Ketterle, Phys. Rev. Lett. **97**, 030401 (2006).
[20] G. B. Partridge, W. Li, Y. A. Liao, R. G. Hulet, M. Haque, and H. T. C. Stoof, Phys. Rev. Lett. **97**, 190407 (2006).
[21] S. Nascimbene, N. Navon, K. J. Jiang, F. Chevy, and C. Salomon, Nature **463**, 1057 (2010).
[22] N. Navon, S. Nascimbene, F. Chevy, and C. Salomon, Science **328**, 729 (2010).
[23] F. Chevy and C. Mora, Rept. Prog. Phys. **73**, 112401 (2010).
[24] W. V. Liu and F. Wilczek, Phys. Rev. Lett. **90**, 047002 (2003).
[25] S.-T. Wu and S. Yip, Phys. Rev. A **67**, 053603 (2003).
[26] I. Shovkovy and M. Huang, Phys. Lett. B **564**, 205 (2003).
[27] P. F. Bedaque, H. Caldas, and G. Rupak, Phys. Rev. Lett. **91**, 247002 (2003).
[28] W. V. Liu, F. Wilczek, and P. Zoller, Phys. Rev. A **70**, 033603 (2004).
[29] J. Carlson and S. Reddy, Phys. Rev. Lett. **95**, 060401 (2005).
[30] M. Mannarelli, G. Nardulli, and M. Ruggieri, Phys. Rev. A **74**, 033606 (2006).
[31] K. Gubbels, M. Romans, and H. Stoof, Phys. Rev. Lett. **97**, 210402 (2006).
[32] D. E. Sheehy and L. Radzihovsky, Phys. Rev. Lett. **96**, 060401 (2006).
[33] L. He, M. Jin, and P. Zhuang, Phys. Rev. D **74**, 036005 (2006).
[34] M. Kitazawa, D. H. Rischke, and I. A. Shovkovy, Phys. Lett. B **637**, 367 (2006).
[35] M. M. Parish, F. M. Marchetti, A. Lamacraft, and B. D. Simons, Nature Physics **3**, 124 (2007).
[36] P. Nikolić and S. Sachdev, Phys. Rev. A **75**, 033608 (2007).
[37] M. M. Parish, F. M. Marchetti, A. Lamacraft, and B. D. Simons, Phys. Rev. Lett. **98**, 160402 (2007).
[38] K. B. Gubbels and H. T. C. Stoof, Phys. Rev. Lett. **100**, 140407 (2008).
[39] L. He and P. Zhuang, Phys. Rev. B **79**, 024511 (2009).
[40] L. Radzihovsky and D. E. Sheehy, Reports on Progress in Physics **73**, 076501 (2010).
[41] K. Gubbels and H. Stoof, Phys. Rept. **525**, 255 (2013).
[42] J. Braun, J.-W. Chen, J. Deng, J. E. Drut, B. Friman, et al., Phys. Rev. Lett. **110**, 130404 (2013).
[43] J. Berges, N. Tetradis, and C. Wetterich, Phys. Rept. **363**, 223 (2002).
[44] H. Gies, Lect. Notes Phys. **852**, 287 (2012).

[45] B.-J. Schaefer and J. Wambach, *Phys.Part.Nucl.* **39**, 1025 (2008).

[46] J. M. Pawłowski, *Annals of Physics* **322**, 2831 (2007).

[47] B. Delamotte, *Lect.Notes Phys.* **852**, 49 (2012).

[48] P. Kopietz, L. Bartosch, and F. Schütz, *Introduction to the Functional Renormalization Group* (Springer, Berlin, 2010).

[49] W. Metzner, M. Salmhofer, C. Honerkamp, V. Meden, and K. Schonhammer, *Rev. Mod. Phys.* **84**, 299 (2012).

[50] J. Braun, *J.Phys.* **G39**, 033001 (2012).

[51] L. von Smekal, *Nucl. Phys. B - Proc. Suppl.* **228**, 179 (2012).

[52] B.-J. Schaefer, *Phys.Atom.Nucl.* **75**, 741 (2012).

[53] M. M. Scherer, S. Floerchinger, and H. Gies, *Phil. Trans. R. Soc. A* **368**, 2779 (2011).

[54] I. Boettcher, J. M. Pawłowski, and S. Diehl, *Nucl. Phys. B - Proc. Suppl.* **228**, 63 (2012).

[55] P. Jakubczyk, W. Metzner, and H. Yamase, *Phys. Rev. Lett.* **103**, 220602 (2009).

[56] P. Strack and P. Jakubczyk, *Phys. Rev. X* **4**, 021012 (2014).

[57] U. Ellwanger and C. Wetterich, *Nucl. Phys.* **B423**, 137 (1994).

[58] D. Jungnickel and C. Wetterich, *Phys. Rev.* **D53**, 5142 (1996).

[59] J. Berges, D. Jungnickel, and C. Wetterich, *Phys. Rev. D* **59**, 034010 (1999).

[60] B.-J. Schaefer and J. Wambach, *Nucl. Phys.* **A757**, 479 (2005).

[61] T. K. Herbst, J. M. Pawłowski, and B.-J. Schaefer, *Phys.Lett.* **B696**, 58 (2011).

[62] T. K. Herbst, J. M. Pawłowski, and B.-J. Schaefer, *Phys. Rev. D* **88**, 014007 (2013).

[63] D. T. Son and M. A. Stephanov, *Phys. Rev. Lett.* **86**, 592 (2001).

[64] P. de Forcrand, PoS **LAT2009**, 010 (2009), arXiv:1005.0539 [hep-lat].

[65] K. Kamikado, N. Strodthoff, L. von Smekal, and J. Wambach, *Phys.Lett.* **B718**, 1044 (2013).

[66] N. Strodthoff, B.-J. Schaefer, and L. von Smekal, *Phys. Rev.* **D85**, 074007 (2012).

[67] T. D. Cohen, (2004), arXiv:hep-ph/0405043 [hep-ph].

[68] D. Ebert and K. Klimenko, *J.Phys.* **G32**, 599 (2006).

[69] D. Roscher, J. Braun, and J. E. Drut, *Phys. Rev.* **A89**, 063609 (2014).

[70] J. Braun, J. E. Drut, T. Jahn, M. Pospiech, and D. Roscher, *Phys. Rev.* **A89**, 053613 (2014).

[71] M. Buballa and S. Carignano, (2014), arXiv:1406.1367 [hep-ph].

[72] H. C. Krahl, S. Friederich, and C. Wetterich, *Phys. Rev. B* **80**, 014436 (2009).

[73] J. Braun, S. Finkbeiner, F. Karbstein, and D. Roscher, (2014), arXiv:1410.8181 [hep-ph].

[74] S. Diehl and C. Wetterich, *Nucl. Phys.* **B770**, 206 (2007).

[75] I. Boettcher, J. Braun, T. K. Herbst, J. M. Pawłowski, D. Roscher, and C. Wetterich, (2014), 1409.5070 [cond-mat.quant-gas].

[76] J. Braun and D. Roscher, (in prep. 2014).

[77] J. M. Pawłowski and F. Rennecke, *Phys.Rev.* **D90**, 076002 (2014), arXiv:1403.1179 [hep-ph].

[78] B. Krippa, (2014), arXiv:1407.5438 [cond-mat.quant-gas].

[79] P. Strack, R. Gersch, and W. Metzner, *Phys. Rev. B* **78**, 014522 (2008).

[80] I. Boettcher, J. M. Pawłowski, and C. Wetterich, *Phys. Rev. A* **89**, 053630 (2014).

[81] S. Floerchinger, M. Scherer, S. Diehl, and C. Wetterich, *Phys. Rev. B* **78**, 174528 (2008).

[82] S. Floerchinger, M. M. Scherer, and C. Wetterich, *Phys. Rev. A* **81**, 063619 (2010).

[83] S. Diehl, S. Floerchinger, H. Gies, J. Pawłowski, and C. Wetterich, *Annalen der Physik* **522**, 615 (2010).

[84] I. Boettcher, S. Diehl, J. M. Pawłowski, and C. Wetterich, *Phys. Rev. A* **87**, 023606 (2013).

[85] C. Lobo, A. Recati, S. Giorgini, and S. Stringari, *Phys. Rev. Lett.* **97**, 200403 (2006).

[86] R. Schmidt and T. Enss, *Phys. Rev. A* **83**, 063620 (2011).

[87] N. Navon, S. Nascimbène, X. Leyronas, F. Chevy, and C. Salomon, *Phys. Rev. A* **88**, 063614 (2013).

[88] D. F. Litim, *Nucl. Phys.* **B631**, 128 (2002).